ORIGINAL ARTICLE

Validation of in Vivo Myocardial Strain with PET Derived Feature Tracking: Direct Comparison with Tagging-Cine Magnetic Resonance

Masataka Katahira, MD[1)], Kenji Fukushima, MD, PhD[2)], Keiichiro Endo, MD, PhD[1)], Masateru Kawakubo, PhD[3)], Naoyuki Ukon, PhD[4)], Ryo Yamakuni, MD[2)], Takatoyo Kiko, MD, PhD[1)], Takeshi Shimizu, MD, PhD[1)], Shiro Ishii, MD, PhD[2)], Masayoshi Oikawa, MD, PhD[1)], Michinobu Nagao, MD, PhD[5)], Hiroshi Ito, MD, PhD[2)], and Yasuchika Takeishi, MD, PhD[1)]

Received: January 25, 2025 / Revised manuscript received: March 5, 2025 / Accepted: March 28, 2025
J-STAGE advance published: May 8, 2025

Abstract

***Purpose*: The aim of this study was to validate positron emission tomography feature tracking (PETFT) for assessing endocardial wall strain by comparing it with conventional tagging-cine magnetic resonance (MR) derived strain analysis (TAG).**

***Methods*: Consecutive 62 patients who underwent ^{13}N-ammonia PETMR (52 males, mean age 66 years) were enrolled. PETFT and TAG were obtained through simultaneous acquisition with electrocardiography-gated PET and cine-MR for rest scan. Global longitudinal and circumferential strain (GLS and GCS) were calculated. Correlations and Bland-Altman plots were employed to evaluate associations, bias, and 95% limit of agreement (LOA) between PETFT and TAG.**

***Results*: PETFT and TAG showed significant correlations (r=0.69 [95% CI: 0.54 to 0.80], p<0.0001; r=0.55 [95% CI: 0.33–0.80], p < 0.0001 for GCS and GLS, respectively). Bland-Altman plot showed acceptable agreements (Bias 0.7 ± 6.7, LOA -12.5 to 13.9; Bias 1.3 ± 5.5, LOA -9.5 to 12.0 for GCS and GLS, respectively). In patients with abnormal perfusion, the correlations were still significant (r=0.76 [95% CI: 0.62 to 0.93], p<0.0001; r=0.59 [95% CI: 0.18 to 0.82], p=0.007 for GCS and GLS, respectively).**

***Conclusion*: PETFT has been identified as a feasible technique compared to TAG, demonstrating its potential as a novel tool for assessing wall strain in routine clinical practice. However, discrepancies in strain values may arise due to differences in algorithms and the presence of perfusion defects.**

Keywords: Cardiac magnetic resonance, Coronary artery disease, Feature tracking, Myocardial strain, Positron emission tomography, Tagging cine
Ann Nucl Cardiol 2025; 11 (1): 26–32

Assessment of left ventricular (LV) function is a mainstay of the diagnosis and management in patients with coronary artery disease. LV ejection fraction (LVEF) has played a pivotal role in the risk stratification and prognostic implication. Among various non-invasive imaging modalities, nuclear imaging technique has a significant advantage, allowing stress testing in clinical routine. However, LVEF is a simplified index of volume change calculated from end-diastolic and end-systolic volumes, making it difficult to detect abnormalities in patients with preserved LVEF. Hence, there is a need for a novel index that enables to visualize and quantify the LV functional abnormalities in more detail, even

DOI: 10.17996/anc.25-00002

1) Department of Cardiovascular Medicine, Fukushima Medical University School of Medicine, Fukushima, Japan
2) Department of Radiology and Nuclear Medicine, Fukushima Medical University School of Medicine, Fukushima, Japan
3) Department of Health Sciences, Faculty of Medical Sciences, Kyushu University, Fukuoka, Japan
4) Advanced Clinical Research Center, Fukushima Medical University, Fukushima, Japan
5) Department of Diagnostic Imaging and Nuclear Medicine, Tokyo Women's Medical University, Tokyo, Japan

in the cases with preserved LVEF (1). Myocardial strain, a dimensionless index of myocardial deformation, described as the interrelate in three directions of myocardial fiber in LV including circumferential, longitudinal, or radial (2). Strain has been initially reported using the speckle-tracking technique with echocardiography. In current clinical practice, it is widely performed using cardiac magnetic resonance (MR) with feature tracking technique (FT). The algorithm of FT is designed to analyze the endocardial border displacement during cardiac cycle and allows semi-automatic calculation with satisfactory reproducibility. The analysis with FT is available for standard steady-state free precession cine-MR images and does not require additional scan or prolonged post processing (2). We previously developed positron emission tomography (PET) derived FT and validated using hybrid PETMR to compare directly with MR (3). Although FT is most used technique worldwide, other myocardial strain analysis such as tagging-cine (TAG), displacement encoding with stimulated echoes, strain-encoded MR imaging, and fast-strain-encoded MR imaging are also available, and significant differences in measured strain values have been observed among these various technique (4). TAG has been historically considered as the gold standard technique for strain analysis, placing non-physical stripes or grids inside the myocardium and track during cardiac cycle. The imaging technique is fundamentally different from that of FT, demonstrating higher reproducibility among these strain analysis (4, 5). In addition, a novel framework for strain analysis using mapping technique with TAG and machine leaning has been preliminarily validated (6,7). Therefore, a comparison between PETFT and conventional TAG is considered as a useful investigation to introduce PET-derived strain analysis into clinical practice. We aimed to validate PETFT by direct comparison with TAG using hybrid PETMR system.

Methods

Patients

This is a single center, an analysis for prospective observational PET study in our institution (IRB No. 2019-045). We enrolled 67 consecutive patients who underwent rest-pharmacological stress ^{13}N-ammonia PET/MR for known or suspected coronary artery disease. This study was approved by the institutional review board of Fukushima Medical University, and all the participants were given the written informed consent. The patients who had poor image quality including motion artifacts that did not allow for reliable tracking were excluded. The patient demographics such as history and cardiovascular risk factors were retrieved from the patients' medical records at the time of the PET scan.

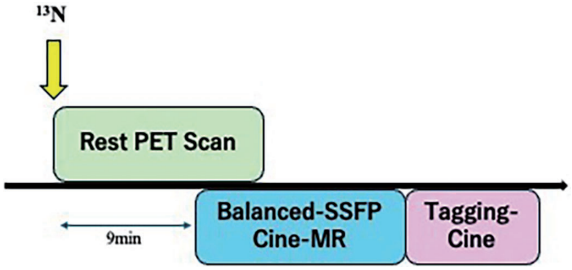

Figure 1
Rest ^{13}N-ammonia PETMR protocol is shown. ^{13}N-ammonia was administrated at a time of starting list-mode PET scan. After the interval of the half-life of perfusion agent (approximately 9 min), breath-hold cine-MR with balanced steady-state free precession (SSFP). Tagging-cine (TAG) was conducted immediately after SSFP cine.

Hybrid PETMR acquisition protocol

PET and MR scan were simultaneously performed using a hybrid PETMR system (Biograph mMR, Siemens Healthineers, Erlangen, Germany). Figure 1 shows PETMR acquisition protocol. We employed the rest scan for the comparison between PETFT and TAG through rest-stress PETMR because the acquisition duration for stress scan was limited by the administration of vasodilator, unavailable to allow additional time for TAG. As previously reported, the attenuation map was calculated from a standard Dixon-based attenuation correction prior to the PET scan. A bolus of ^{13}N-ammonia (500–700 MBq) was injected with saline flushes. A 14-minute list-mode scan was performed (8, 9). The imaging data were reconstructed using a 3D attenuation-weighted ordered-subset expectation maximization iterative reconstruction algorithm with three iterations and 21 subsets. The images were smoothed with a 2-mm full width at half maximum Gaussian filter. The image data matrix was 172 × 172, with a pixel size of 3.42 mm and a slice thickness of 2.03 mm. ECG gated PET images with 16-frame were analyzed using commercially available software (Corridor 4DM®, INVIA, Ann Arbor, MI, USA) to obtain LVEF, LV end-diastolic, and end-systolic volume (LVEDV, LVESV, respectively). Cine MR with electrocardiographic-gated balanced steady-state free cine sequences was performed immediately after the rest PET scan, followed by electrocardiographic-gated, expiring breath-holding TAG cine acquisition. MR acquisition and post-processing were performed based on the guidelines of the Society of Cardiac Magnetic Resonance (10). Short axis slices cine-MR was employed to measure LV volumetry, and LVEF. The following parameters were applied: echo time of 1.5 ms, repetition time of 3.4 ms, matrix of 256 × 256 pixels, flip angle of 50°, and typical field-of-view of 350 mm. The repetition time was automatically adjusted according to the patient's heart rate. The acquisition parameters for TAG were follows: echo time of 3.2 ms, repetition time of 40.9 ms, voxel size 1.4

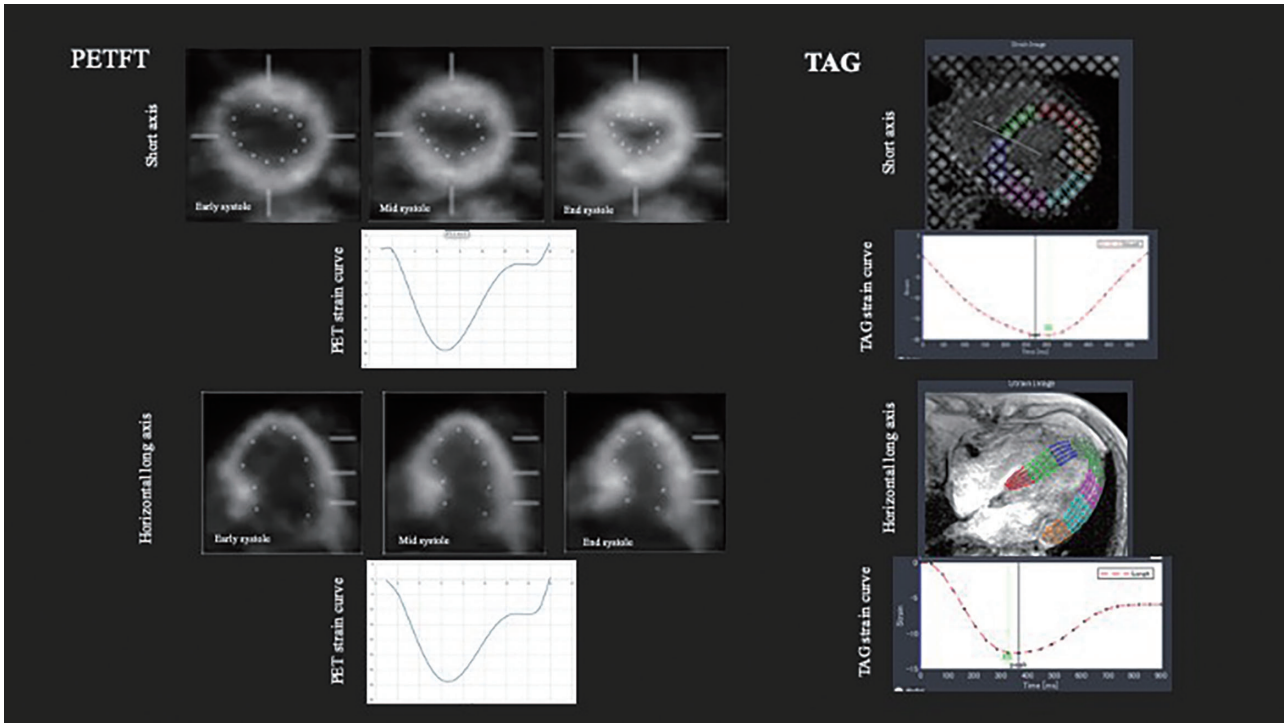

Figure 2

Schematic illustration of PET derived FT, and TAG are shown. PET cine images for short axis, and long axis view were imported as a video format. The endomyocardial contour was manually tracked on endo-diastole, and automatically tracked during whole cardiac cycle using in-house original application based on Matlab® (left). The analysis for TAG was performed using dedicated commercially available software (Segment®) (right). Similar to PET, the endomyocardial contour was manually tracked on endo-diastole, and automatically tracked from endo-diastole to endo-systole.

× 1.4 × 7.0 mm, flip angle of 12°, and 8 phases per cycle. LVEDV, LVESV, and LVEF were calculated using a dedicated commercially available software with semi-automatic calculation (Segment®, MEDVISO, Lund, Sweden) as previously reported (3).

PETMR strain analysis

Figure 2 shows schematic images of strain analysis for PETMR. Gated PET cine images of horizontal long, vertical long, and 3 slices (basal, middle, apex) short axis (SA) were imported as movie format to be implemented using MATLAB R2020a (version 9.8; Mathworks Inc., Natick, MA, USA). The endocardial border was manually defined and traced on the cine images at end-diastole, and were automatically tracked during a cardiac cycle, using a local template-matching technique based on normalized correlation coefficient values, as previously described to obtain global longitudinal strain (GLS), and those from the SA were as global circumferential strain (GCS) (11). Inter-observer and intra-observer reproducibility for PETFT was previously validated (3). Strain analysis for TAG was performed using semi-automatic calculation with Segment® (Figure 2B). End and epicardial wall contour were manually traced at endo-diastolic phase, and were automatically tracked for whole cardiac cycle to obtain GLS for averaged value from a horizontal long (4ch)- and a vertical long (2ch)-axis; GCS for averaged value from 3 slices of SA for basal, middle, and apical slice.

Statistical analysis

Data are presented as the mean ± standard deviation (SD) or number and percentage (%). Statistical analyses were performed using PRISM® version 9 (Graph pad Inc., NY, USA), with $p < 0.05$ considered statistically significant. Pearson's correlation coefficients (r) with 95% confidence interval (CI) of strain values between PET and MR were calculated for linearly and non-linearly distributed data. Fisher's z-test was employed to evaluate the significance of differences between independent correlation coefficients. Bland-Altman plot was used to compare the obtained strain values, and bias, SD, and 95% limit of agreement (LOA) were determined (12). Linear regression analysis for the mean and the difference was additionally performed if a proportional error was observed.

Results

PETFT of 5 patients revealed poor image quality and were not available for strain analysis. Three patients had lower radioactive counts for gated cine images, resulting failure of

Table 1 Patient demographics (n=62)

Age, years old	65.8 ± 14.5	Post MI, n (%)	21 (32.8)
Male, n (%)	52 (79.1)	Post PCI, n (%)	40 (58.7)
Body mass index, kg/m^2	21.5 ± 3.4	Post CABG, n (%)	6 (10.0)
Hypertension, n (%)	45 (67.2)	Vessels	
Diabetes, n (%)	32 (51.6)	0, n (%)	6 (9.0)
Dyslipidemia, n (%)	52 (77.6)	1, n (%)	18 (26.9)
Smoking, n (%)	39 (58.2)	2, n (%)	22 (35.8)
CKD, n (%)	25 (37.3)	3, n (%)	16 (28.4)
FH, n (%)	9 (13.4)		

CKD, indicates chronic kidney disease; FH, family history of coronary disease; MI, myocardial infarction; PCI, percutaneous coronary intervention; CABG, coronary artery bypass grafting.

Table 2 PETMR parameters

				p
PET-parameters		*MR-parameters*		
Defect score	5.4 ± 6.8			
LVEF (%)	50.7 ± 18.2	LVEF (%)	48.4 ± 16.3	ns
LVEDV (mL)	128.2 ± 57.8	LVEDV (mL)	139.0 ± 46.7	ns
LVESV (mL)	72.0 ± 58.1	LVESV (mL)	77.1 ± 48.9	ns
GLS	-12.1 ± 5.3	GLS	-12.4 ± 4.2	ns
Horizontal strain	-12.6 ± 5.7	*Horizontal strain*	-12.5 ± 4.4	ns
Vertical strain	-13.5 ± 6.3	*Vertical strain*	-11.9 ± 4.2	ns
GCS	-17.7 ± 9.6	GCS	-15.8 ± 6.1	ns

LVEF, left ventricular ejection fraction; LVEDV, LV end-diastolic volume; LVESV, LV end-systolic volume; GLS, global longitudinal strain; GCS, global circumferential strain

Table 3 Correlation between PET and MR strain

	r	95%CI	p
GLS	0.55	0.54 to 0.80	<0.0001
Horizontal strain	0.49	0.27 to 0.72	0.0004
Vertical strain	0.77	0.57 to 0.87	<0.0001
GCS	0.69	0.54 to 0.80	<0.0001

GLS, global longitudinal strain; GCS, global circumferential strain

wall-tracking, and 2 patients showed a significant liver uptake. Consequently 62 patients were included. Table 1 shows the patients demographics. Mean age was 66 years old, and 52 were male. More than half of the participants have a history of coronary intervention, and nearly 30% had a multi vessel disease. Table 2 shows the functional parameters obtained from PETMR study. The average defect score was 5.4 and ranged from 0 to 24. The abnormal rest perfusion (summed defect score ≥4) was observed for 22 patients. The volumetric and functional parameters including LVEF and strain values did not show a significant difference between PET and MR. Table 3 shows the correlation of strain values between PETFT and TAG. In the strain analysis for long axis strain, the horizontal, vertical, and GLS (the average of long axis strain) demonstrated a significant correlation. In the circumferential strain, GCS showed a significant correlation. Figure 3 shows representative plots of the correlation and Bland-Altman analysis for GLS and GCS between PETFT and TAG. PETFT and TAG showed significant correlations (r=0.69 [95% CI: 0.54 to 0.80], p<0.0001; r=0.55 [95% CI: 0.33–0.80], p< 0.0001 for GCS and GLS, respectively). Bland-Altman plot showed acceptable agreements, while a significant proportional error was observed (Bias 0.7 ± 6.7, LOA -12.5 to 13.9, r= -0.4, and p=0.002; Bias 1.3 ± 5.5, LOA -9.5 to 12.0, r=-0.5, and p < 0.0001 for GCS and GLS, respectively). Figure 4 shows the plots in patients with abnormal perfusion (defect score≥4, n=22), the correlations were still significant (r=0.76 [95% CI: 0.62 to 0.93], p<0.0001; r=0.59 [95% CI: 0.18 to 0.82], p = 0.007 for GCS and GLS, respectively). Figure 5 shows two representative cases for PETFT and TAG. A

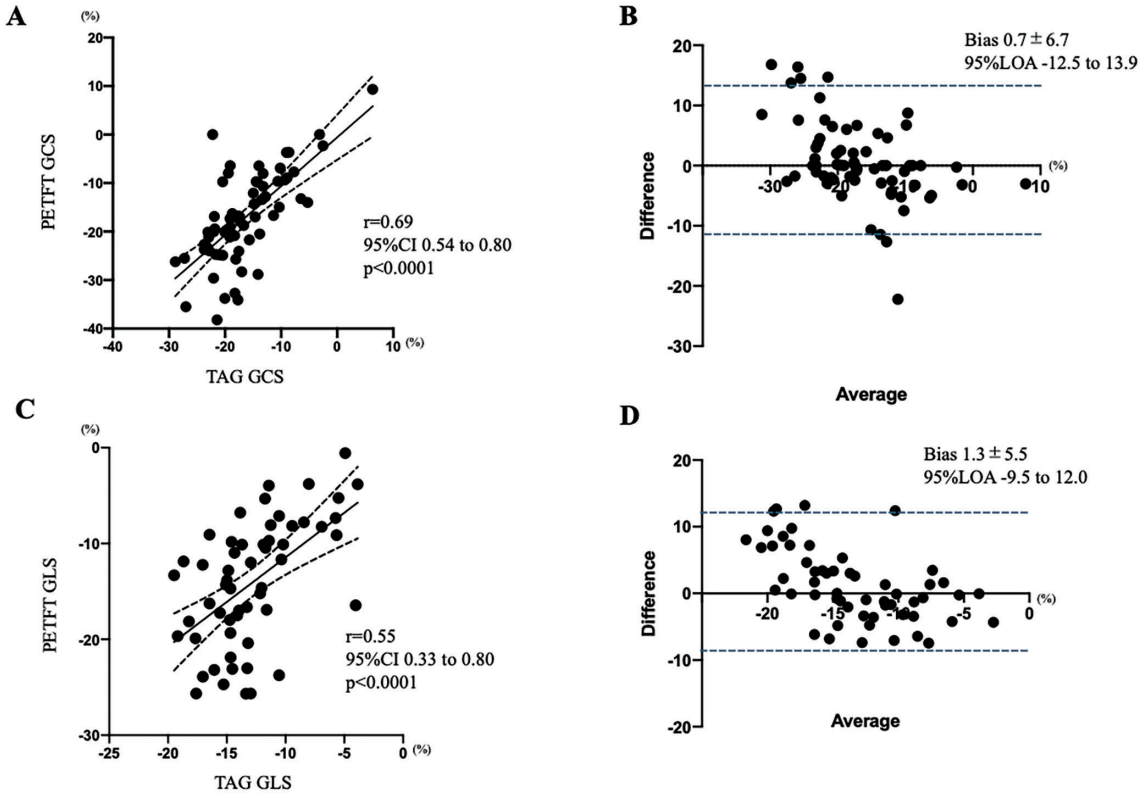

Figure 3

The correlation analysis and Bland-Altman plots for GCS and GLS are shown. PETFT and TAG showed significant correlations (r = 0.69 [95% CI: 0.54 to 0.80], p < 0.0001; r = 0.55 [95% CI: 0.33–0.80], p < 0.0001 for GCS and GLS, respectively) (A and C). Bland-Altman plot showed acceptable agreements, while a significant proportional error was observed (Bias 0.7 ± 6.7, LOA -12.5 to 13.9, r=-0.42, and p=0.002; Bias 1.3 ± 5.5, LOA -9.5 to 12.0, r=-0.49, and p<0.0001 for GCS and GLS, respectively) (B and D).

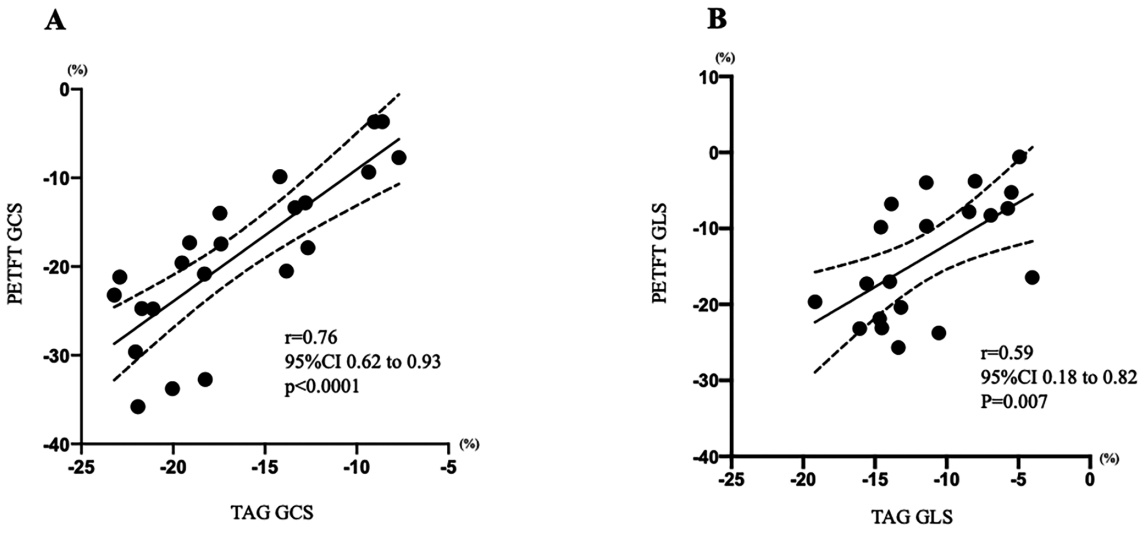

Figure 4

The correlation analysis for GCS (A) and GLS (B) in patients with abnormal perfusion (defect score≥4, n=22) are shown. Both GCS and GLS showed a significant correlation between PETFT and TAG (r=0.76 [95% CI: 0.62 to 0.93], p<0.0001; r =0.59 [95% CI: 0.18 to 0.82], p=0.007 for GCS and GLS, respectively).

illustrates the case with normal perfusion and function (defect score = 0, and rest PET-LVEF 66%). GCS were -20.1 and -23.0; GLS were -17.6 and -14.1 for PETFT and TAG respectively. B illustrates the case with a history of anterior infarction, demonstrating a significant anterior defect and reduced LV function (defect score = 8, and rest PET-LVEF 47%). GCS were -17.2 and -12.7; GLS were -7.8 and -8.4 for PETFT and TAG respectively.

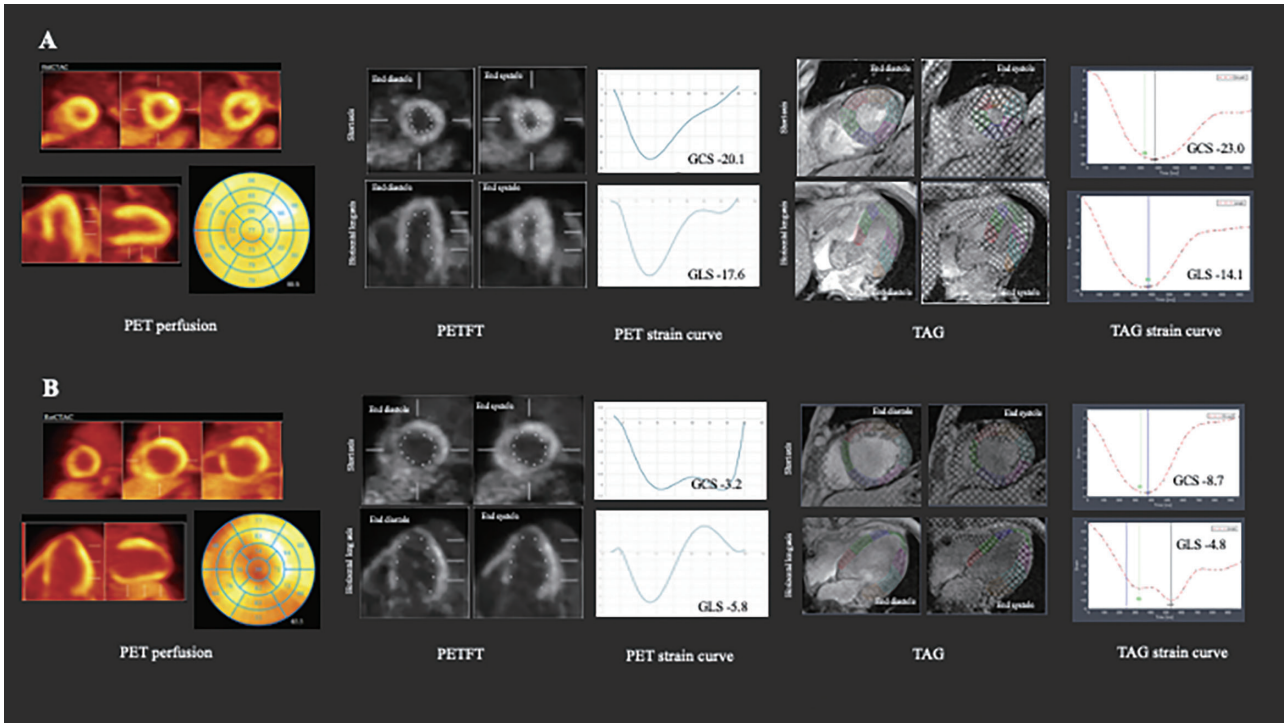

Figure 5

Two representative cases for PETFT and TAG are shown. A illustrates the case with normal perfusion and function (defect score=0, and rest PET-LVEF 66%). GCS were -20.1 and -23.0; GLS were -17.6 and -14.1 for PETFT and TAG respectively. B illustrates the case with a history of anterior infarction, demonstrating a significant anterior defect and reduced LV function (defect score=8, and rest PET-LVEF 47%). GCS were -17.2 and -12.7; GLS were -7.8 and -8.4 for PETFT and TAG respectively.

Discussion

The present study validated PETFT parameter with conventional TAG in clinical practice. Both GLS and GCS showed a significant correlation and demonstrated acceptable agreement for Bland-Altman plots with a significant proportional error. In patients with perfusion defects, the correlation was still significant for both GCS and GLS. The original investigation of PETFT from our study was developed using PET cine images with time-of-flight technique (11). However, as previously reported, PETFT showed a significant correlation with MR-FT with and without time-of-flight (3, 13). The results of previous studies have indicated that the PETFT analysis has a significant potential to be more widely introduced into routine clinical practice. Numerous studies using MR and echocardiography have suggested that strain can serve as an independent index distinct from conventional LVEF and may also be useful for prognostic assessment (14). Considering the strength of routine nuclear imaging in providing the functional information under stress, PETFT may have an incremental impact on diagnostic and prognostic performance over conventional functional assessment such as LVEF, diastolic parameters, and phase analysis. The reason we did not conduct the comparison between PETFT and TAG for stress scan is that the pharmacological stress agent we generally use has a short biological half-life, limiting to perform various MR sequence during stress scan (15).

The differences in the wall tracking algorithm between PETFT and TAG should be discussed: the tracking algorithm of the endomyocardial wall is fundamentally different between them. PETFT is a perfusion-based template matching technique for endomyocardial contour tracking, and is therefore influenced by the endomyocardial or transmural defects (11). On the other hand, TAG directly implants non-physical marker as grid lines on myocardium and track them during early to end systole, namely the transmural myocardium was tagged and not influenced by the perfusion defect (16). Although there was a significant positive correlation, Bland-Altman analysis revealed a significant proportional error for both GCS and GLS. Possible reasons of this error are follows: the detection of endomyocardial border is far different because it is significantly influenced by spatial resolution and the size of tagged grid in TAG. The inferior spatial and temporal resolution may result in underestimating the LV size during systole. In the patients with reduced function and dilated LV cavity, PETFT tracking may overestimate the LV size. The difference in acquisition conditions should be discussed. PETFT was conducted during free-breathing state, whereas TAG was performed in expiring breath-hold technique, which may influence on wall motion,

particularly in the inferior wall. The number of phases obtained in each cardiac cycle was 8 in TAG, and the number of bins obtained in each cardiac cycle was 16 in PET. As previously discussed, it is speculated that the location of perfusion defect may impact on PETFT analysis (e. g the defect in basal area may cause the error in endomyocardial contour tracking). In addition, misregistration is also one of the possible causes of the error. The registration is challenging because the axis orientation was performed separately for PET and TAG acquisition, and the gated PET analysis using 4DM® has been fully automated. Therefore, we did not perform regional analysis such as coronary territory in the present study. Although the echocardiography and MR have been a robust and established technique for strain, the results of our study indicated the clinical utility of PETFT as a robust technique in clinical routine.

Conclusion

PETFT has been identified as a feasible technique compared to TAG, highlighting its potential as a novel tool for assessing wall strain in routine clinical practice. However, discrepancies in strain values may arise due to differences in algorithms and the presence of perfusion defects.

Acknowledgments

None.

Sources of funding

This study was supported in part by JSPS-Kakenhi (grant no. 22K07701) to KF.

Conflicts of interest

No other potential conflict of interest relevant to this article was reported.

Reprint requests and correspondence:
Kenji Fukushima MD, PhD.
Department of Radiology and Nuclear Medicine, Fukushima Medical University School of Medicine, Fukushima, 1 Hikarigaoka, Fukushima 960-1295, Japan.
E-mail: kfukush4@fmu.ac.jp

References

1. Yuasa N, Obokata M, Harada T, et al. Characterization and prognostic importance of chronotropic incompetence in heart failure with preserved ejection fraction. J Cardiol 2024; 83: 113–20.
2. Yang W, Xu J, Zhu L, et al. Myocardial strain measurements derived from MR feature-tracking: Influence of sex, age, field strength, and vendor. JACC Cardiovasc Imaging 2024; 17: 364–79.
3. Katahira M, Fukushima K, Endo K, et al. Feasibility of position emission tomography derived endocardial wall strain: Direct comparison with magnetic resonance using hybrid ^{13}N ammonia PETMR system. Ann Nucl Med 2025; 39: 285–94.
4. Bucius P, Erley J, Tanacli R, et al. Comparison of feature tracking, fast-SENC, and myocardial tagging for global and segmental left ventricular strain. ESC Heart Fail 2020; 7: 523–32.
5. Lardo AC, Abraham TP, Kass DA. Magnetic resonance imaging assessment of ventricular dyssynchrony: Current and emerging concepts. J Am Coll Cardiol 2005; 46: 2223–8.
6. Cao JJ, Ngai N, Duncanson L, Cheng J, Gliganic K, Chen Q. A comparison of both DENSE and feature tracking techniques with tagging for the cardiovascular magnetic resonance assessment of myocardial strain. J Cardiovasc Magn Reson 2018; 20: 26.
7. Hammouda K, Khalifa F, Abdeltawab H, et al. A new framework for performing cardiac strain analysis from cine MRI imaging in mice. Sci Rep 2020; 10: 7725.
8. Endo K, Kiko T, Yamakuni R, et al. Prognostic value of simultaneous analysis with myocardial flow reserve and right ventricular strain by hybrid ^{13}N-ammonia positron emission tomography / magnetic resonance imaging in coronary artery disease. Int Heart J 2022; 63: 1063–9.
9. Fukushima K, Endo K, Yamakuni R, et al. Simultaneous assessment of left ventricular mechanical dyssynchrony using integrated ^{13}N-ammonia PETMR system: Direct comparison of PET phase analysis and MR feature tracking. J Nucl Cardiol 2023; 30: 1947–58.
10. Kramer CM, Barkhausen J, Bucciarelli-Ducci C, Flamm SD, Kim RJ, Nagel E. Standardized cardiovascular magnetic resonance imaging (CMR) protocols: 2020 update. J Cardiovasc Magn Reson 2020; 22: 17.
11. Kawakubo M, Nagao M, Yamamoto A, et al. ^{13}N-ammonia positron emission tomography-derived endocardial strain for the assessment of ischemia using feature-tracking in high-resolution cine imaging. J Nucl Cardiol 2022; 29: 2103–14.
12. Gerke O. Reporting standards for a bland-altman agreement analysis: A review of methodological reviews. Diagnostics (Basel) 2020; 10: 334.
13. Kawakubo M, Nagao M, Kikuchi N, et al. ^{13}N-ammonia positron emission tomography-derived left-ventricular strain in patients after heart transplantation validated using cardiovascular magnetic resonance feature tracking as reference. Ann Nucl Med 2022; 36: 70–81.
14. Smiseth OA, Rider O, Cvijic M, Valkovič L, Remme EW, Voigt J-U. Myocardial strain imaging: Theory, current practice, and the future. JACC Cardiovasc Imaging 2025; 18: 340–81.
15. Yamamoto A, Nagao M, Kawakubo M, et al. Prediction of cardiovascular events using myocardial strain ratio derived from ^{13}N-ammonia positron emission tomography. Eur Radiol 2023; 33: 3889–96.
16. Ibrahim El-SH. Myocardial tagging by cardiovascular magnetic resonance: Evolution of techniques--pulse sequences, analysis algorithms, and applications. J Cardiovasc Magn Reson 2011; 13: 36.